Comparison on the Seismic Demand Spectrum Using Seismic Data From Taipei Basin

Chin-Hsiung Loh and Chau-Shen Hwang

Department of Civil Engineering, National Taiwan University, Taipei, Taiwan, R.O.C.

Jeng-Yaw Hwang

Seismological Observation Center, Central Weather Bureau, Taipei, Taiwan, R.O.C.

Abstract

A large number of earthquake data have been recorded after the operation of Taiwan Strong Motion Instrumentation Program. The purpose of this paper is to use these recorded accelerogram to study the seismic demand for single-degree-of-freedom system. From the analysis one can assess the importance of different demand parameters and evaluate patterns in demand parameters that will improve our understanding of the physical phenomena involved in seismic response of structures. The following demand parameters are analyzed:

(1) Inelastic Strength Demand: Strength demand are expressed as a base shear coefficient. It represents yield level over seismically effective weight. To limit the ductility ratio the period dependent yield level is calculated. The inelastic strength demand spectrum is developed.

(2) Strength Reduction Factor: The strength reduction factor is the ratio of the elastic strength demand imposed on a SDOF system to the inelastic strength demand for a specific target ductility ratio. It shows how much the yield level capacity of a given elastic SDOF system can be reduced.

Comparison on the seismic demand spectrum is made using the seismic data from Taipei basin. Effects of source directivity, basin effect and local site conditions on the seismic demand spectrum are discussed. Besides the seismic response of Taipei basin is also studied which include the principal direction of wave passage in the basin, distribution of PGA, spectra ratio and response spectrum in the basin.

1 Introduction

There is increasing evidence that strong seismic ground motion amplified through soil layers overlying "base" rock can produce surface motions having effects on structures that are much stronger than implied in most building codes. A recent case history was offered by the September 19, 1995 Michoacan, Mexico earthquake which cause imprecedented destruction in Mexico City (Seed, *et al.*, 1987). The effects of site amplifications were also observed during the 1989 Loma Prieta, California, earthquake (Benuska, 1990) and the 1995 Kobe earthquake (JGS, 1996). As more ground motion data are collected, the local geological site conditions appear to be the dominant factor for controlling the variation in ground motion (Aki, 1988; Janpe *et al.*, 1988; Finn 1991). The possibility that the local site conditions influence the amplitudes of recorded seismic waves in sediment-filled valleys or in basins have also been investigated by many researchers (Abrachamson

& Bolt, 1987; Rosenblueth, 1992; Wen *et al.*, 1995). The results show that local soil conditions can significantly affect the characteristics of ground motion during earthquakes. These papers were based on the objectives to determine the various kinds of sites on the forces to be used in the design of structures to resist strong seismic ground motion and the primary concern is the determination of site amplification which can be applied to the code design forces.

Taipei city is the capital of Taiwan. It is located on a sediment-filled basin. The concept of the assessing seismic ground motion hazard of this area requires both quantifying the predicted ground motion at a specific location within this basin and assigning an error (or site amplification factor) associated with this prediction because of the basin effect. The goal of the proposed study is to study the observed variation of site amplification from three different earthquake motions across this basin and discuss the site response with the seismic source on the response spectra and the seismic demand spectrum within the basin so that the basin effect can be considered in the design code. The analysis includes:

(1) perform the principal direction analysis and the response spectral analysis in order to find the correlation of local site amplification with seismic source;

(2) discuss the seismic demand spectrum which include constant ductility spectrum and strength demand spectrum over the whole basin area.

2 Gelogy and the Strong Motion Observation Network

The area of the Taipei basin with an altitude below 20 meter is about 24 km^2. The basin is filled with unconsolidated sediments. The contour line of the depth of the base rock surface is shown in Fig. 1. The deepest place of the base rock surface, about 250 meters in depth, is located on west side of the basin. The geological structure inside the basin consists of the quaternary layers above the tertiary base rock. Table 1 shows the P-wave velocity structure of the basin. The stratigraphic formations of the quaternary layers are, in descending order, surface soil, the Sungshan formation, the Chingmei formation and the Hsinchung formation. The Sungshan formation is composed of alternating beds of silty clay and silty sand and covers almost the whole Taipei basin. The Chungmei formation is a fan-shaped body of conglomeratic deposits. The Hsinchuang formation consists of bluish grey, clayey sand with conglomerate beds (Wen, 1995).

Under the Taiwan Strong Motion Instrumentation Program (TSMIP), executed by the Seismological Observation Center of the Central Weather Bureau, Taiwan, R. O. C., a total of forty-three stations are already in operation on the free-field of the Taipei basin area. The instrumentation is a force-balanced three-component accelerometer with a 16-bit resolution which makes the apparatus capable of recording high-resolution ground motion within $\pm$ 2g and with a pre-event and post-event memory. The distribution of instrumentation is shown in Fig. 2 and indicated by triangle symbols. In this figure, the dotted lines show the contours of the depth with same level of base rock.

After the operation of TSMIP several events that triggered by this Taipei basin strong motion observation network. Three events with magnitude greater than 6.0 and triggered most of the array network of Taipei basin were selected for the study of basin site amplification. These three events are: June 5, 1994, with magnitude of 6.57 and depth of 5.3 km; June 25, 1995, with magnitude of 6.50 and depth of 39.8 km; and March 5, 1996, with magnitude 6.5 and depth of 15.9 km. The epicenters of these three earthquakes are indicated in Fig. 3. The hypocenter of 1994-6-5 earthquake located in shallow zone and the hypocenter of 1995-6-25 earthquake located in deep zone.. From the distribution of aftershocks of these three events, the rupture length of the 1994-6-5 earthquake can be identified as a fault-rupture source model with rupture length of 30 km in the direction of east-west direction. The identified rupture length of this event is close to the rupture length-magnitude relationship of Taiwan area (i.e., $L(\text{rupture length}) = \exp(1.006\,M - 3.232)$). The 1995-6-25 earthquake was identified as a point source because the distribution of aftershocks is close together.

3 Ground Motion Characteristics of Basin Effects

Because of the deep overlying deposits in the Taipei basin earthquake induced ground motion may have significant influence on the surface ground motion characteristics. In this section the following analyses are performed based on the seismic data recorded from the seismic observation network of Taipei basin for earthquakes of June 5, 1994, June 25, 1995 and March 5, 1996. The analyses include: principal direction analysis, distribution of peak ground acceleration and response spectrum analysis.

Analysis of Principal Direction

In the beginning the principal direction of the recorded ground motion from these three earthquakes in the Taipei basin was calculated. Using frequency window, given a frequency band, the variance-covariance matrix of the three-orthogonal ground acceleration recorded at each station is calculated first, and the direction of principal axes are the eigenvectors derived from the covariance matrix (Loh, 1985). Major principal direction is determined from the eigenvector which corresponds to the major eigenvalue. Figure 4 shows the major principal axis calculated from these three events between the frequency band of 1.0 Hz $\sim$ 1.4 Hz. It is found that major principal axes of ground motion from observation network at Taipei basin are almost in horizontal direction and the major principal direction for June 25, 1995 earthquake is more consistent in all stations within the basin than the other two earthquakes. It is believed that the June 25, 1995 earthquake is a deep earthquake with a more like point source model than the other two earthquakes so the result of principal direction analysis shows more consistent.

Distribution of Peak Ground Acceleration and Spectral Acceleration

The contour of the PGA distribution of these three events for north-south motion is shown in Fig. 5. It is found that the shape of contour for 1994-6-5 and 1996-3-5 earthquakes looks similar and the shape of contour for 1995-6-25 earthquake is different from the others. The contour of spectral acceleration at $T = 1.0$ sec is also shown in Figs. 6a and 6b for motion in north-south direction and east-west direction, respectively. As compare to the PGA contour map shown in Fig. 5 the contour shapes of spectral acceleration at $T = 1.0$ sec look similar to the PGA contour map. It is concluded that the distribution of PGA as well as the spectral acceleration in the basin strongly depend on the earthquake source characteristics, such as source type, magnitude, and focal depth.

Spectral Ratio Analysis

To compute the spectra ratios of the response spectra (pseudo-acceleration, $S_a(T, 0.05)$) for 5% of critical damping, the mean response spectrum of Taipei basin was first calculated as a reference spectrum, and then the spectral ratio between the response spectrum from the record at each station in the Taipei basin and the calculated mean response spectrum in the same direction was calculated. Figures 7a and 7b show the contour map of spectra ratio at period of 1.6 seconds from these two events. It is found that the spectra ratio does show good correlation between these two events. For both of the two earthquakes larger spectral ratios were observed on the west side of the basin. It means that the amplification of spectral acceleration is greater as compared to the mean spectral acceleration on the west side of the basin. The effect of the soil depth may have significant influences on this spectra ratio. To discuss the design spectra of Taipei basin, the ratios of response spectra were also computed for June 5, 1994 earthquake at each station in the Taipei basin relative to the Taipei basin design spectra. Figure 8 shows the contour map of spectra ratio at period of 1.0 second. In this contour map it shows that some area in the basin with ratio greater than 1.0. It indicates that the current design spectra did not quite conservative especially on the west portion of the basin. Only the June 5, 1994 earthquake has such a phenomenon. For longer period, such as 1.6 sec, this spectral ratios are all smaller than one. The spectral ratio (with respect to design code) is smaller than 1.0 in all periods for the June 25, 1995 earthquake.

4 Inelastic Response Spectra

In this section, attention has been paid to the

inelastic behavior of structures and the benefits gained from their available ductility in aseismic design. The concept of inelastic response spectra was first introduced by Veletsos *et al.* (1965) and Newmark *et al.* (1969), Later Newmark and Hall (1973) proposed a procedure where a set of factors can be formulated in terms of the ductility of a system. Recently, Pal *et al.* (1987) developed yield displacement spectra, constant strength spectra, and constant ductility spectra using different hysteresis model.

The main objective of this study is to examine the site-dependent inelastic spectra for various yield levels by using the earthquake data recorded at the Taipei basin.

The equation of motion of a single degree of freedom nonlinear system is given as follows:

$$m\,\ddot{x}(t) + c\,\dot{x}(t) + R(t) = -m\,\ddot{y}(t) \qquad (3)$$

where m is the mass of the system, c is the viscous damping coefficient, R is the restoring force, x is the displacement of the mass relative to the base, and $\ddot{y}$ is the ground absolute acceleration. The viscous damping is assumed to be proportional to the mass of the system. Equation (10) can be rewritten as

$$\frac{\ddot{x}(t)}{x_y} + 2\,\xi\,\omega\,\frac{\dot{x}(t)}{x_y} + \frac{R(t)}{m\,x_y} = -\frac{\ddot{y}(t)}{x_y} \qquad (4)$$

in which x_y is the yield displacement of the system, and ξ is the system damping ratio and ω is the natural frequency of the system $\omega = \sqrt{k/m}$. Let $\mu = x(t)/x_y$, and rearrange the $R(t)/m\,x_y$ and $\ddot{y}(t)/x_y$ as follows [Mahin *et al.*, 1983]:

$$\left.\begin{aligned} &\frac{R(t)}{m\,x_y} = \frac{K}{m}\,\frac{R(t)}{K\,x_y} = \omega^2\,\frac{R(t)}{R_y} = \omega^2\,\rho(t) \\ &\frac{\ddot{y}(t)}{x_y} = \frac{K}{m}\,\frac{\ddot{y}(t)}{x_y} = \frac{\omega^2\,m\,\ddot{y}(t)}{R_y} \\ &\eta \equiv \frac{R_y}{m\,\ddot{y}_{\max}} \end{aligned}\right\} \qquad (5)$$

in which R_y is the yield force of the system, and x_y is the yield displacement of the system. β is defined as the strength factor and it expresses the systems's yield strength relative to the maximum inertia force of an infinitely rigid system. $\rho(t)$ is the normalized restoring force. Equation (11) can be rewritten as

$$\ddot{\mu}(t) + 2\,\omega\,\xi\,\dot{\mu}(t) + \omega^2\,\rho(t) = -\frac{\omega^2\,\ddot{y}(t)}{\beta\,\ddot{y}_{\max}} \qquad (6)$$

From this one can determine numerically the maximum ductility for a particular system with a certain period and yield strength when subjected to earthquake excitation [Loh *et al.*, 1994].

To represent the inelastic response spectra, the reduction factor is generated (R_μ) which is defined as the ratio of the demanded elastic strength $R_y(\mu = 1)$, to the yielding strength demanded when plastic deformation is allowed up to a maximum selected μ_i, $R_y(\mu = \mu_i)$. Figure 9 shows the reduction factor R_μ for different ductility ratio using the data recorded at station TAP37 for 1994-6-5 earthquake. Variation of reduction factor at certain period all over the basin is shown in Fig. 10. It is concluded that a constant value of reduction factor may not be an appropriate value for design in Taipei basin. From Eq. (5), the yield strength demand spectra was normalized with respect to the peak ground acceleration $\ddot{y}$, and expressed as

$$\eta = \frac{R_y}{m\,\ddot{y}_{\max}} = \frac{C_y\,W}{m\,\ddot{y}_{\max}} = \frac{C_y}{\ddot{y}_{\max}\,1\,g} \qquad (7)$$

where C_y is the yielding seismic coefficient. Figure 11 shows the yielding seismic coefficient ($C_y = C/F_u$) as a factor of period.

5 Damage Control Model — Inelastic Analysis

Damage models considering the effect of cumulative energy dissipation are widely used in research of energy-based earthquake-resistant design. The Park and Ang model based on the maximum displacement and total hysteretic energy dissipation is used on the study of seismic demand parameters. It is given by

$$\mathrm{DF} = \frac{\mu_d}{\mu_u}\left(1 + \frac{\beta\,E_H}{R_y\,x_{\max}}\right) \qquad (8)$$

where DF = the damage index (DF < 2 represents slight damage, DF < 0.4 represents moderate damage, DF > 0.4 represents damage beyond repair, and DF > 1.0 represents total collapse), μ_D = ductility demand, μ_u = ultimate ductility capacity, $x_{\max}$ = maximum displacement, E_H = hysteretic energy, β = parameter whose value depends on specific structural characteristics, and R_y = yield strength. In this study

a comprehensive evaluation of demand parameters is performed for elasto-perfect plastic single-degree-of-freedom systems. With the damage control criteria (i.e., DF-value) the objectives of the study are: (a) to assess the importance of different demand parameters, (b) to provide statistical information on demand parameters that can be utilized to assess the performance of structures designed according to existing code. The damage control criteria is defined as the calculation of demand parameters under the assumption of a specific value of DF in Park and Ang model (DF = 1.0 in this study). The demand parameters are represented in terms of spectra of strength reduction factors and inelastic strength demand spectra. Because of the implement of the specific damage model the demand parameters will include not only the maximum displacement but also the total hysteretic energy dissipation. Based on Eq. (8) the yield strength R_y can be expressed as a function of DF, β, μ_u and the structural system parameters. Under the assumption of DF = 1.0 and a suitable β-value, R_y can be calculated with a specified μ_u. The reduction factor as well as yielding seismic coefficient can also be constructed. It indicated that the seismic coefficient may be different due to different value of damage index and β-value.

From the seismic data collected from different site conditions in Taipei basin the analysis include: (a) Effects of maximum ductility demand capacity on strength reduction factor and on inelastic strength demand spectra for different site conditions; (b) Effects of damage factor (DF-value in Park and Ang model) on demand parameters for different site conditions; (c) Discuss the present results with the seismic design code in Taiwan. Figure 11 shows the calculated yielding seismic coefficient from data recorded at different site. The damage control model was used with $\beta = 0.4$ and DF = 1.0. The code value for Taipei basin is also shown for comparison. Figure 12 shows the variation of β-value on the calculation of yielding seismic coefficient.

6 Conclusions

This research paper performed the ground motion analysis from seismic response data collected from the Taipei basin. Three particular earthquakes, June 5, 1994 earthquake, June 25, 1995 earthquake, and March 5, 1996 earthquake were selected for the analysis in this study. Because of the entirely differences of the three seismic sources (the 1995-6-25 earthquake is the deep earthquake and it looks similar to a point source while the 1994-6-5 earthquake is a shallow earthquake with line source) the site amplification in the basin are quite different. Through the analyses the following conclusions are drawn:

(1) The major principal directions calculated from the 1995-6-25 earthquake response of Taipei basin strong motion array are quite similar in their principal direction at frequency range 1.0 Hz to 1.4 Hz. Since the seismic source of this earthquake is located at deep zone and can be identified as point source and the waves propagated vertically from underlying base rock to surface is obvious, then identified principal direction is similar from all the stations. The 1994-6-5 earthquake is a shallow earthquake more complicate on the wave propagation as waves cross the basin. The identified principal direction is not so consistent.

(2) The distribution of PGA and response spectra in the basin is different from event to event. For the microzonation study of ground motion of the basin one must consider the source effect as one of the important factors to the seismic response of basin.

(3) From the study of yield strength demand spectra significant difference was observed from seismic data of different site. From the result of Fig. 11, it is clear that the depth of soil deposit has significant influence on the evaluation of yielding seismic coefficient. The data of 1994-6-5 earthquake data shows that for deeper soil deposit the yielding seismic coefficient is greater than the code value in the longer period. It has to be pointed out different β-value means different types of structural system. If β-value did not equal to zero, the hysteretic energy of the response was considered in the analysis, and the yielding seismic coefficient is larger for the larger β-value.

Acknowledgements

The research project was supported by National Science Council under Grant No. NSC86-

2621-P-002-024 and Central Weather Bureau. The authors wish to express their thanks for this research grants.

References

1. Benuska, K. L., "Source Lessons learned from the 1989 Loma Prieta, California earthquake," Proceedings, 4th US National Conference on Earthquake Engineering, Vol. 1, 1990, pp. 91–105.

2. Seed, H. B., Romo, M. P., Sun, J., Jaime, A. and Lysmer, J., "Relationship Between Soil Conditions and Earthquake Ground Motions in Mexico City in the Earthquake of September 19, 1985," Report UCB/EERC 87/15, Earthquake Engineering Research Center, University of California, Berkeley, CA, 1987.

3. Japanese Geotechnical Society, Soils and Foundation – Special Issue on Geotechnical Aspects of the Jan. 17, 1995 Hyogoken-Nambu Earthquake.

4. Aki, K., "Local Site Effects on Strong Ground Motion," Earthquake Engineering and Soil Dynamics II – Recent Advances in Ground-Motion Evaluation, J. L. von Thun (Editor), ASCE, Geotech. Special Publication, No. 20, 1988, pp. 103–155.

5. Jarpe, S. P., Cramer, C. H., Tucker, B. E. and Shakal, A. F., "A Comparison of Observations of Strong Ground Response to Weak and Strong Motion at Coalinga, California," Bull. Seism. Soc. Am., 78, 1988, pp. 421–435.

6. Finn, W. D. Liam, "Geotechnical Engineering Aspects of Microzonation,"' Proceeding of 4th Int. COnf. on Seismic Zonation, Vol. 1, EERI, Oakland, 1991, pp. 199–259.

7. Abrahamson, N. A. and B. A. Bolt, "Array Analysis and Synthesis Mapping of Strong Seismic Motion," in B. A. Bolt (Editor), Strong Motion Synthesis: Computational Techniques Series, Academia Press, New York, 1987.

8. Rosenblueth, E. and A. Arciniega, "Response Spectra Ratio," Earthquake Engineering and Structural Dynamics, 21, 1992, pp. 483–492.

9. Loh, C. H., Y. T. Yeh, W. Y. Jean and Y. H. Yeh, "Seismic Hazard Analysis in Taiwan: Based on PGA and Spectral Acceleration Attenuation Formula," Int. J. of Engineering Geology, 30, 277–304, 1991.

10. Wen, K. L., Peng, H. T. and Lin, L. F., "Basin Effects Analysis from a Dense Strong Motion Observation Network," Earthquake Engineering and Structural Dynamics, 24, 1995, pp. 1069–1083.

11. Mahin, S. A. and J. Lin, "Construction of Inelastic Response Spectra for Single-Degree-of-Freedom System," UCB/EERC 83/17, University of California, Berkeley, June, 1983.

12. Newmark, N. M. and W. J. Hall, "Design Criteria for Nuclear Reactor Facilities," *Proc. 4th World Conference On Earthquake Engineering*, Santiago, Chile, Vol. II, pp. B-4, IAEE, 1969, pp. 37–50.

13. Newmark, N. M. and W. J. Hall, "Procedures and Criteria for Earthquake Resistant Design, Building Practices for Disaster Mitigation," *National Bureau of Standards*, Vol. BSS-46, 1973, pp. 209–236.

14. Pal, S., S. S. Dasaka, and A. K. Jain, "Inelastic Response Spectra," *Computer and Structures*, Vol. 25, No. 3, 1987, pp. 335–344.

15. Veletsos, A. S., N. m. Newmark, and C. V. Chelapati, "Reformation Spectra for Elastic and Elasto-Plastic Systems Subjected to Ground Shock and Earthquake Motions," Proc. 3rd World Conference on Earthquake Engineering, New Zealand, Vol. II, IAEE, 1965, pp. 663–680.

16. Jean, W. Y., "A Study on Seismic Design Parameters and Structural Reliability Analysis," Ph.D. Thesis, Department of Civil Engineering, National Taiwan University, July 1996.

Table I. P-wave velocity structure of Taipei Basin[6]

Depth (m)	Layer velocity (m/sec)	Refractor velocity* (m/sec)	Formation
0–10	400	350	Alluvium
10–60	1550	1500	Sungshan
60–120	2050	1260	Chingmei
120–180	2400	2410	Upper Hsinchuang
180–240	3100		Lower Hsinchuang
> 240	3800	3640	Base Rock

*Fong *et al.*[8]

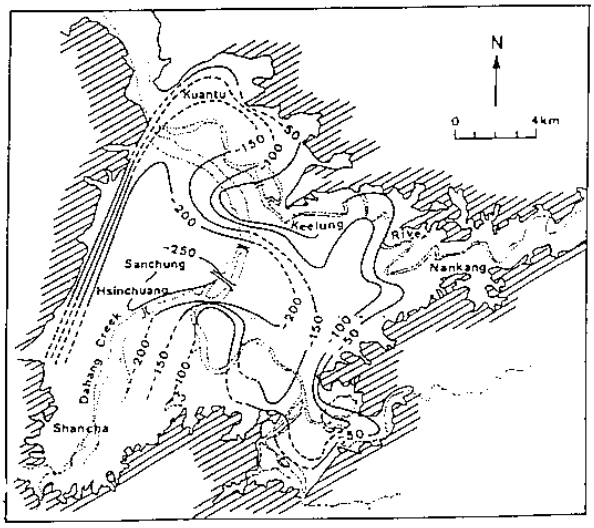

Fig.1: Map of the Taipei basin. The contours indicate the depth of the base rock surface (in meter).

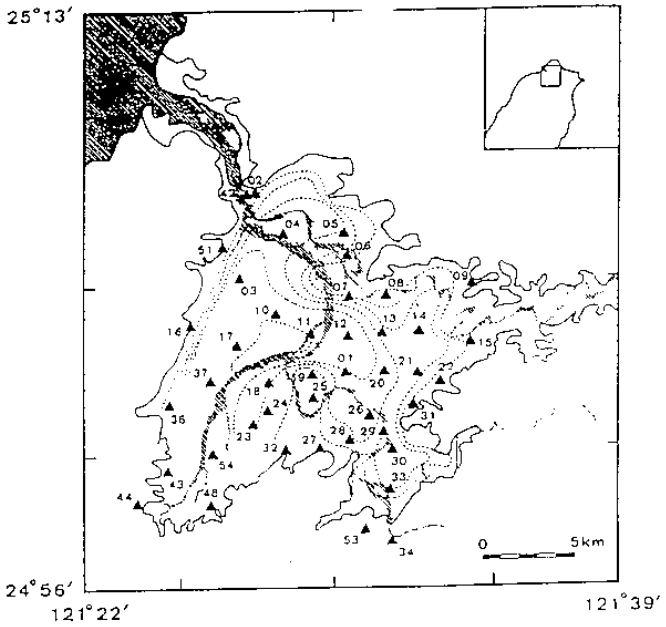

Fig. 2: Strong motion instrumentation locations of the Taipei Strong Motion Observation Network.

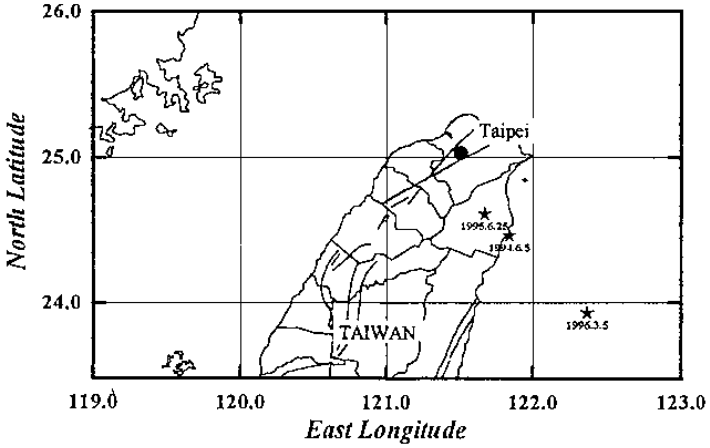

Fig.3: Epicenters of three earthquakes (1994-6-5, 1995-6-25, 1996-3-5).

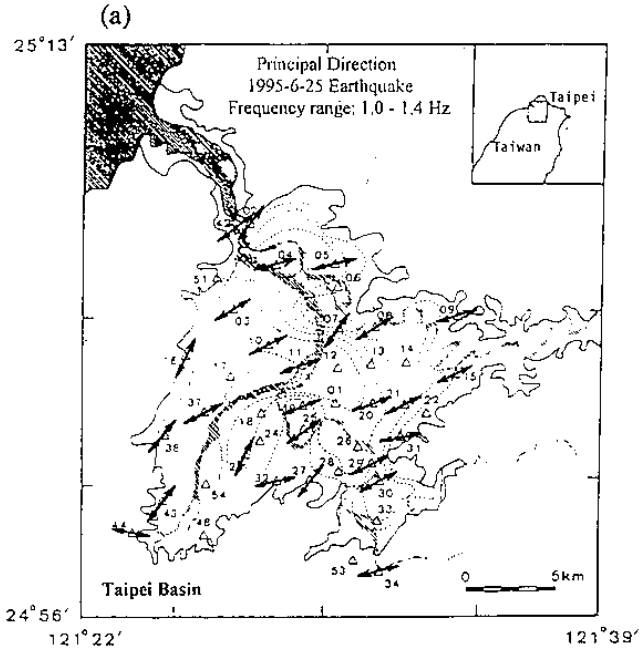

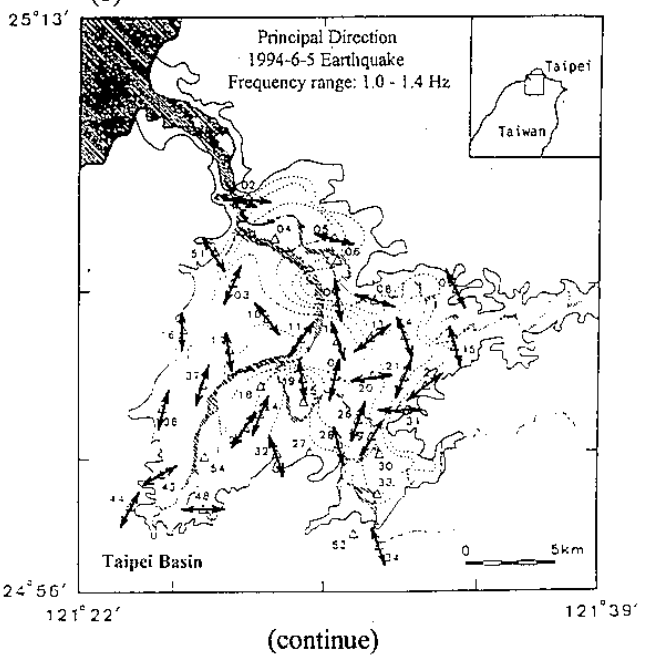

(continue)

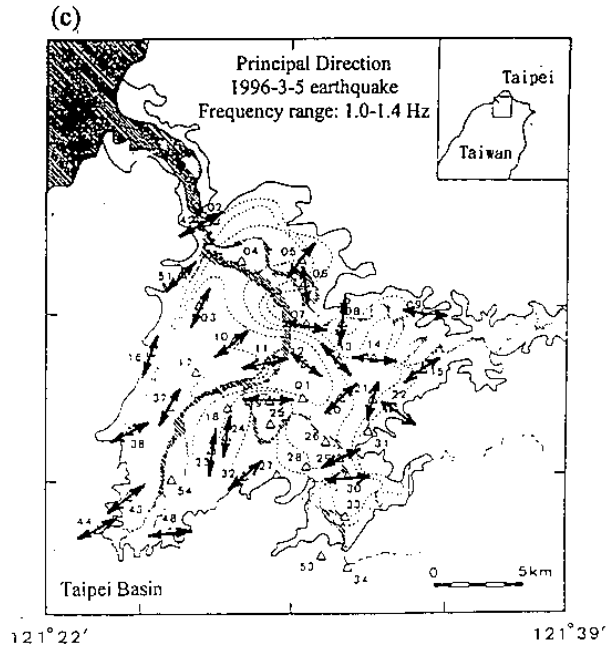

Fig.4a: Major principal direction in the frequency range between 1.0Hz and 1.4Hz for, (a) 1995-6-25 earthquake, (b) 1994-6-5 earthquake, (c) 1996-3-5 earthquake.

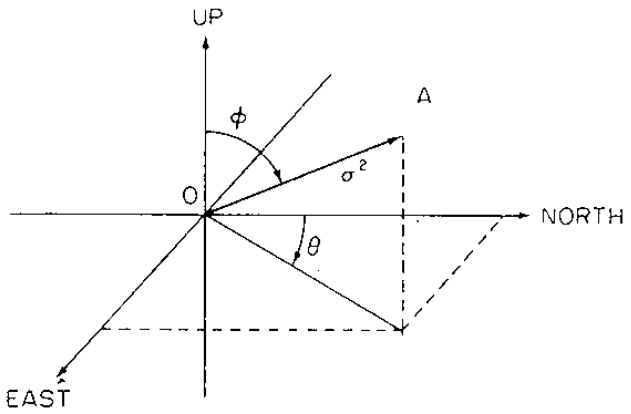

$$\bar{\mu} = \begin{bmatrix} \mu_{xx} & \mu_{xy} & \mu_{xz} \\ \mu_{yx} & \mu_{yy} & \mu_{yz} \\ \mu_{zx} & \mu_{zy} & \mu_{zz} \end{bmatrix}$$

$$\mu_{ij} = \int_{t_0-\frac{1}{2}\Delta t}^{t_0+\frac{1}{2}\Delta t} a_i(\tau)a_j(\tau)\mathrm{d}\tau \quad i,j = x, y, z$$

$$\bar{\mu}_{\mathrm{P}} = [A]^{\mathrm{T}}[\bar{\mu}][A] = \begin{bmatrix} \mu_{x'} & 0 & 0 \\ 0 & \mu_{y'} & 0 \\ 0 & 0 & \mu_{z'} \end{bmatrix}$$

Fig. 4b: Calculation of Principal direction. The mathematical formulation of variance-covariance matrix of ground motion is also shown.

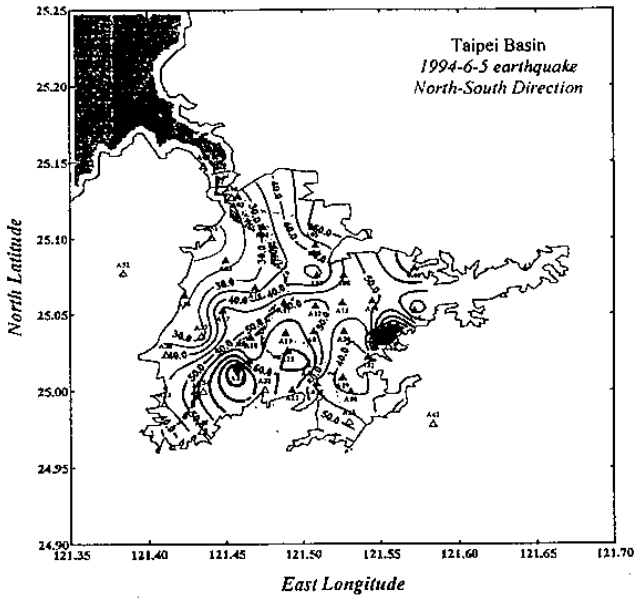

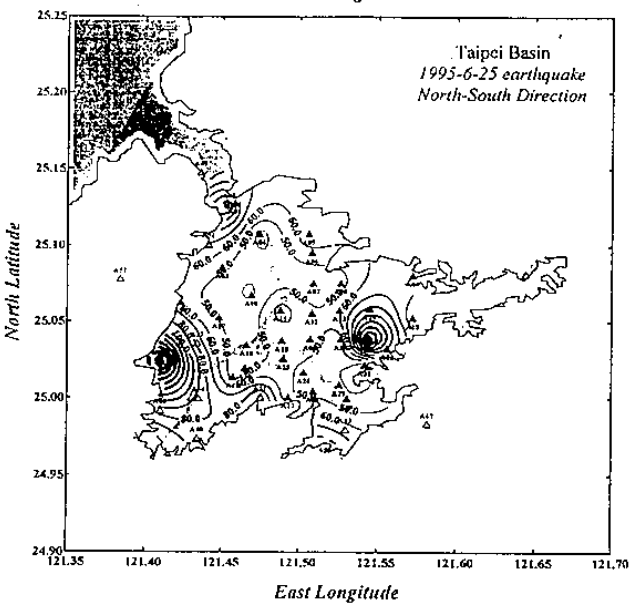

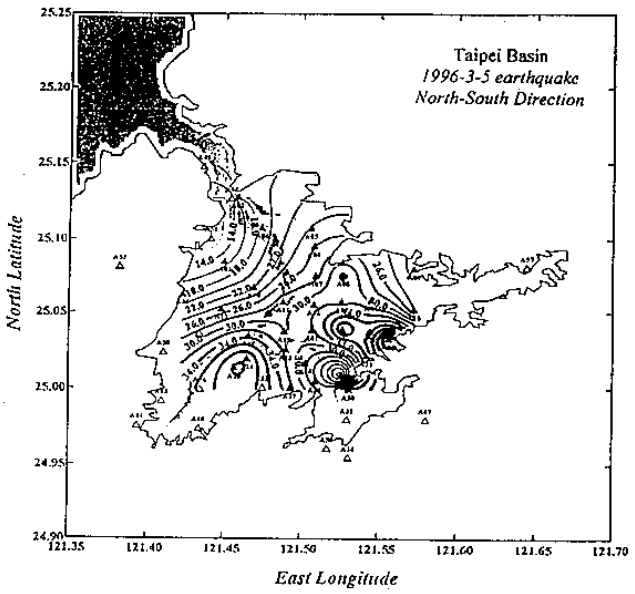

Fig.5: Contour map of peak ground acceleration (unit:g) of Taipei basin for , (a) 1994-6-5 earthquake, (b) 1995-6-25 earthquake, (c) 1996-3-5 earthquake.

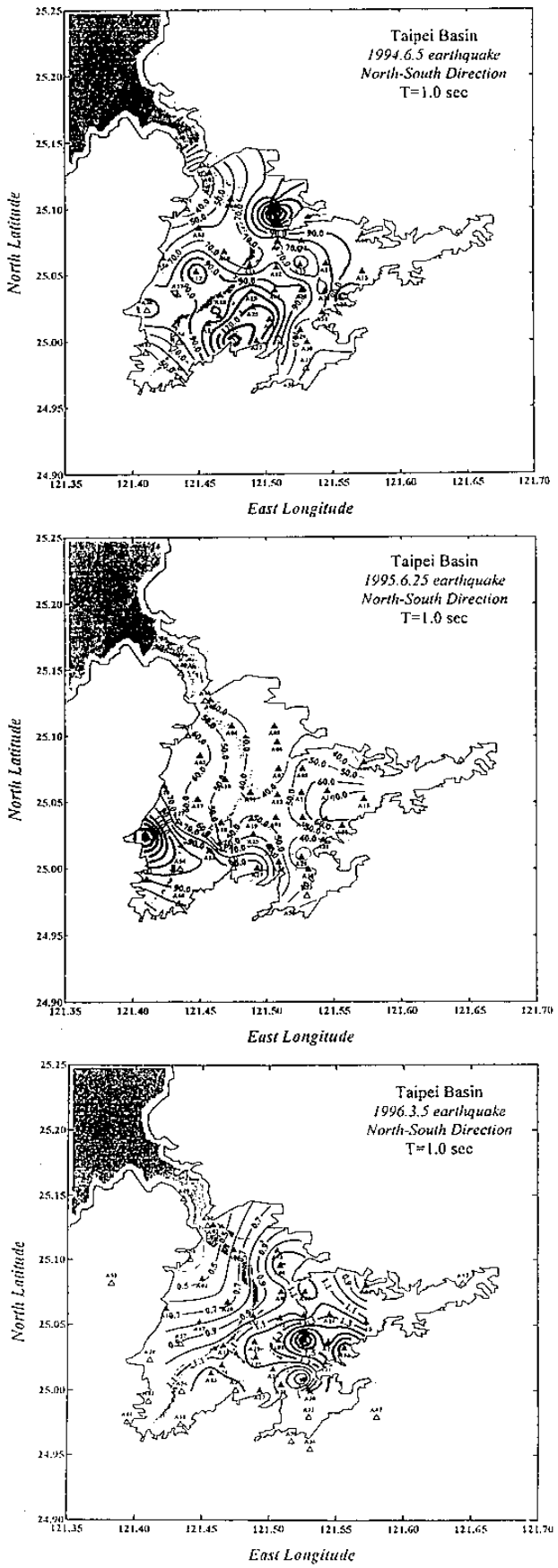

Fig.6: Contour map of spectral acceleration (Sa) at T=1.sec. for earthquake of, (a) 1994-6-5, (b) 1995-6-25, (c) 1996-3-5.

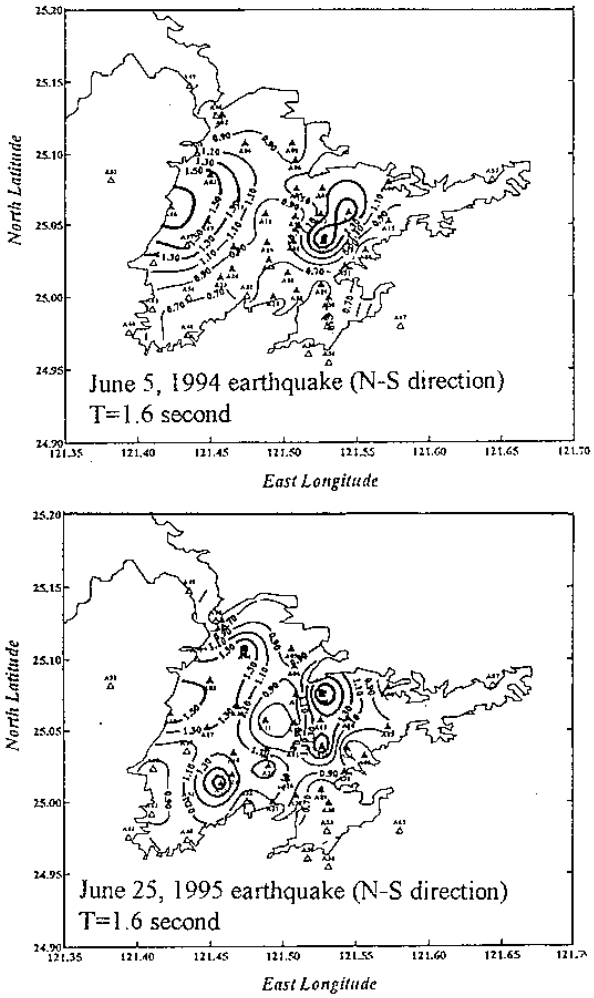

Fig.7: Contour map of spectral ratio (Sa divided by mean value of Sa) at T-1.6 sec. (a) 1994-6-5, (b) 1995-6-25.

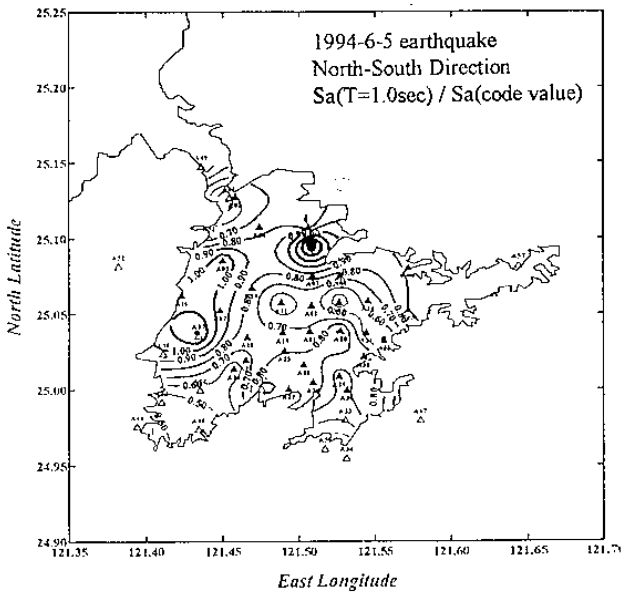

Fig.8: Contour map of spectral ratio (Sa(T-1.sec) / Sa(code)) for 1994-6-5 earthquake.

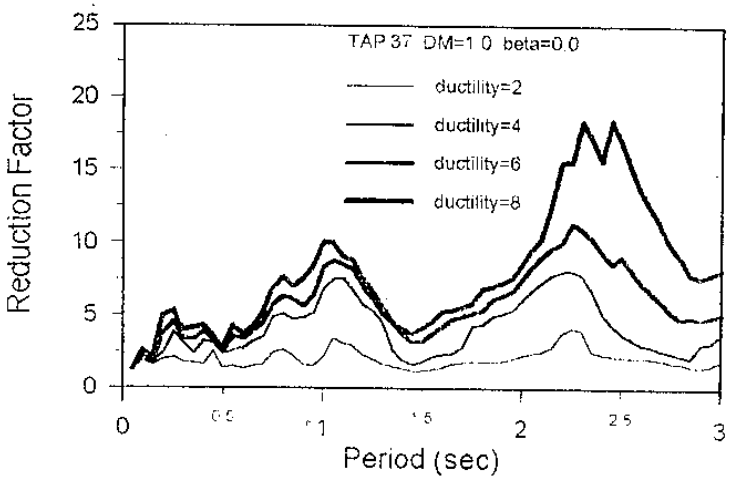

Fig.9: Plot of reduction factor (using EPP model) aas a function of period for different ductility ratio. The 1994-6-5 earthquake at station TAP-37 was used for the analysis.

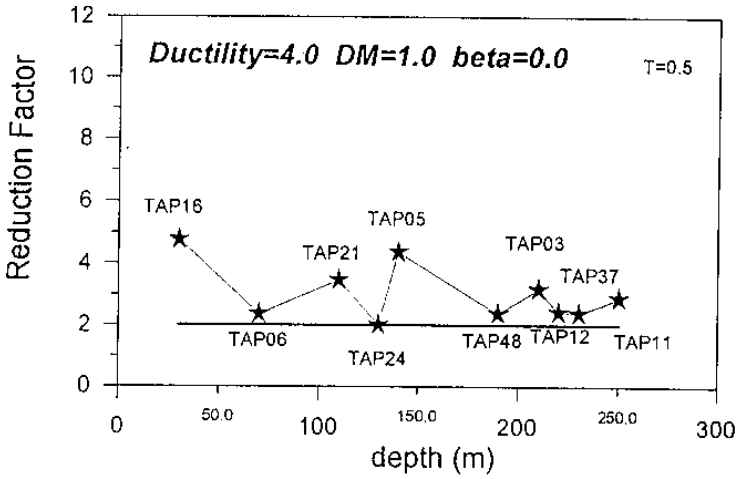

Fig. 10: Variation of reduction factor (for T=0.5 and T=1.2 sec) with respect to the depth of soil deposit (usinf 1994-6-4 earthquake)..

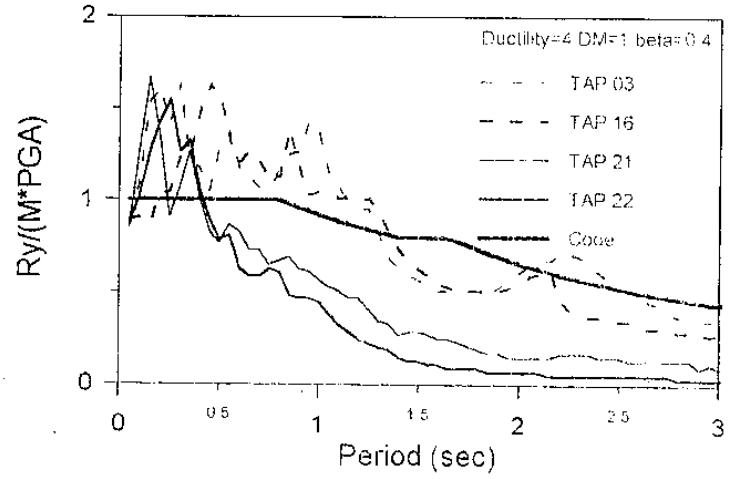

Fig. 11: Effect of the depth of soil deposit to the influence of yielding seismic coefficient (using damage control model: ductility =4.0, beta=o.4, and DF=1.0)

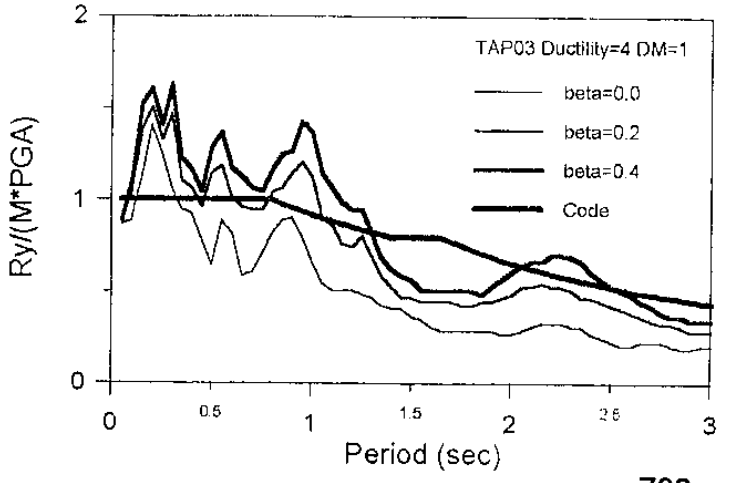

Fig. 12: Effects of beta-value in dmamge control model on the influence of yielding seismic coefficient.